A New Benchmark *In Vivo* Paired Dataset for Laparoscopic Image De-smoking

Wenyao Xia[1], Victoria Fan[1], Terry Peters[1,2,3], Elvis C. S. Chen[1,2,3,4]

[1] Robarts Research Institute, Western University, Canada
[2] School of Biomedical Engineering, Western University, Canada
[3] Department of Medical Biophysics, Western University, Canada
[4] Department of Electrical and Computer Engineering, Western University, Canada

Abstract. The single greatest obstacle in developing effective algorithms for removing surgical smoke in laparoscopic surgery is the lack of a paired dataset featuring real smoky and smoke-free surgical scenes. Consequently, existing de-smoking algorithms are developed and evaluated based on atmospheric scattering models, synthetic data, and non-reference image enhancement metrics, which do not adequately capture the complexity and essence of *in vivo* surgical scenes with smoke. To bridge this gap, we propose creating a paired dataset by identifying video sequences with relatively stationary scenes from existing laparoscopic surgical recordings where smoke emerges. In addition, we developed an approach to facilitate robust motion tracking through smoke to compensate for patients' involuntary movements. As a result, we obtained 21 video sequences from 63 laparoscopic prostatectomy procedure recordings, comprising 961 pairs of smoky images and their corresponding smoke-free ground truth. Using this unique dataset, we compared a representative set of current de-smoking methods, confirming their efficacy and revealing their limitations, thereby offering insights for future directions. The dataset is available at https://github.com/wxia43/DesmokeData.

Keywords: Benchmark dataset · surgical image de-smoking · laparoscopic surgery · dataset creation

1 Introduction

Laparoscopic surgery, with its minimally invasive approach, has significantly transformed patient care by reducing recovery times and minimizing infection risks. However, the smoke generated by electrocautery or laser tools during these procedures poses a substantial challenge, as it obscures the surgical field, potentially increasing the risk of errors and prolonging operation times [1]. While hardware solutions like Laparoshield ™and the ClearFlow Smoke Evacuation System are available, their need for repetitive manual operation is time-consuming, inefficient, and negatively impacts surgeons' performance [7]. A preferred alternative involves digitally removing the appearance of smoke through a *de-smoking* image processing technique, thereby providing surgeons with an unobstructed view of the surgical site *in situ* [21].

A major obstacle in developing surgical image de-smoking algorithms is the scarcity of paired *in vivo* images, consisting of smoky laparoscopic images and their corresponding smoke-free ground truths. As extensively reported in recent literature [21,5,23,17,30], there is currently no *in vivo* paired dataset available for laparoscopic de-smoking. The absence of such a dataset significantly hinders progress in surgical de-smoking research in three key areas.

1. **Development of Suitable Image Models**: Traditional models, such as the atmospheric physical model [11], are designed for outdoor scenes and do not adequately capture the unique characteristics of surgical scenes, including uneven lighting and limited depth. Additionally, surgical smoke has different scattering properties than outdoor haze or fog, leading to secondary reflections and altering scene illumination rather than simply obscuring it [22]. The close proximity and high magnification of the surgical camera make large particles or droplets visible, resulting in a non-uniform smoke distribution across the laparoscopic scene. This could potentially limit the effectiveness and authenticity of creating synthetic data.
2. **Advancement of AI-Based Methods**: To overcome the absence of a paired dataset, AI-based de-smoking algorithms have typically been developed using synthetic data [21,5,23,30] or through unpaired learning approaches [17,12,18,19]. However, models trained solely on synthetic paired images tend to overfit and often generalize poorly [28] to *in vivo* surgical scenes, especially when synthetic data are generated through inaccurate image modelling. In the case of unpaired learning, the lack of direct correspondence between images can lead to suboptimal image restoration [25]. Techniques such as CycleGAN [31] may introduce artifacts and structural distortions, often failing to utilize high-quality information from ground truth for guiding the image restoration process [4]. Furthermore, they can cause colour distortions and detail loss, thereby hindering the application of downstream techniques for surgical image enhancement.
3. **Evaluation and Comparison of Algorithms**: Conducting fair and rigorous evaluations of de-smoking algorithms is challenging without a paired *in vivo* dataset. While non-reference metrics offer an intuitive evaluation of de-smoking results from several image quality perspectives, including contrast, sharpness, and naturalness [9], they are inadequate in determining the presence of image artifacts, the trueness of recovered structural content, and colour fidelity compared to fully referenced metrics. This limitation restricts the quantitative assessment of the efficacy of existing techniques using *in vivo* surgical data, thereby hindering the iterative process of algorithmic improvements. In contrast, referenced metrics set a definitive performance standard, making them indispensable in applications where preserving the original image quality is critical, especially during laparoscopic surgeries.

These scenarios lead to a significant need in the medical imaging community for a paired *in vivo* dataset tailored to laparoscopic surgical de-smoking. To address this need, we present a novel methodology to create the first *in vivo* paired dataset for surgical de-smoking. Our contributions are threefold: 1) Development

of a novel surgical de-smoking dataset, currently comprising 21 scenes with 961 pairs of smoky and smoke-free images, marking the first dataset to offer realistic smoke-free ground truth for surgical scenes, 2) A cost-effective methodology to generate such a paired dataset from existing laparoscopic surgical videos, and 3) Evaluation of eight recent de-smoking algorithms using our dataset, providing a benchmark for future research.

2 Key Challenges

The process of creating such a dataset is impeded by the following challenges:

1. **De-smoking ground truth cannot be manually labelled**: Creating paired datasets in medical imaging often relies on human annotation, with object segmentation being a prime example. Humans excel at recognizing patterns and spatial awareness, which facilitate manual segmentation based on visual cues and feature localization. However, creating ground truth for image restoration tasks, such as de-smoking, involves reconstructing the original, unobstructed image content in its natural appearance. This process requires precise knowledge of the original scene's appearance and the specific degradation effects, which are beyond human capability to accurately recreate without computational assistance.

2. **Efficacy vs. cost trade-off for *ex vivo* simulation**: A feasible, though not ideal, approach involves creating a paired dataset using *ex vivo* tissues by capturing stationary scenes both with and without smoke. One such pioneering effort is from the TMI dataset [10], which includes a sub-dataset comprising 5 pairs of *ex vivo* images of animal abdominal organs under both smoky and smoke-free conditions. However, this method is insufficient for emulating the intricate details of *in vivo* laparoscopic scenes, such as the natural colour of *in vivo* tissues, reflections from bodily fluids, irregular organ surfaces due to surgical cuts and incisions, and the appearance of smoke in a pressurized environment under single-source lighting. While some of these technical challenges could be overcome with sufficient time and resources, the high costs make this methodology impractical for creating large datasets to simulate various surgical scenarios.

3. ***In vivo* data usually contains unpredictable motion**: Similar to the *ex vivo* approach, conducting *in vivo* animal trials while capturing images from simulated surgical procedures may be viable. However, in addition to the issue of cost, which naturally limits the sample size, *in vivo* data often exhibit inherent motion caused by the live subject's breathing, heartbeat, and involuntary muscle movements. Such motion renders the surgical scene dynamic, undermining the strategy of using a smoke-free scene at an early timeframe as the ground truth for subsequent smoky scenes. To solve this problem, dense pixel-based motion correction is required. However, developing a tracking algorithm capable of operating under heavy vision obstructions, such as surgical smoke, remains a significant challenge [8].

3 Dataset Creation

The premise of our approach to creating a paired dataset, *i.e.* identical scenes *with* and *without* surgical smoke, is the recognition of the existence of nearly stationary scenes during surgery when the smoke is about to emerge. Concretely, the moment immediately before and after the cauterization tool is activated, the spatial arrangements of the surgical scene are nearly identical, but the image sequence captured immediately after cauterization contains surgical smoke. Their spatial arrangement contains subtle differences, perturbed possibly by the camera, surgical tool, and involuntary anatomical motion. To ensure the creation of a paired dataset with identical spatial arrangement, we further apply a motion correction technique to align the paired images. To address each type of motion, our method is divided into two stages: 1) Candidate video clip selection and large motion rejection, and 2) Small motion correction and paired data refinement.

3.1 Candidate video clip selection

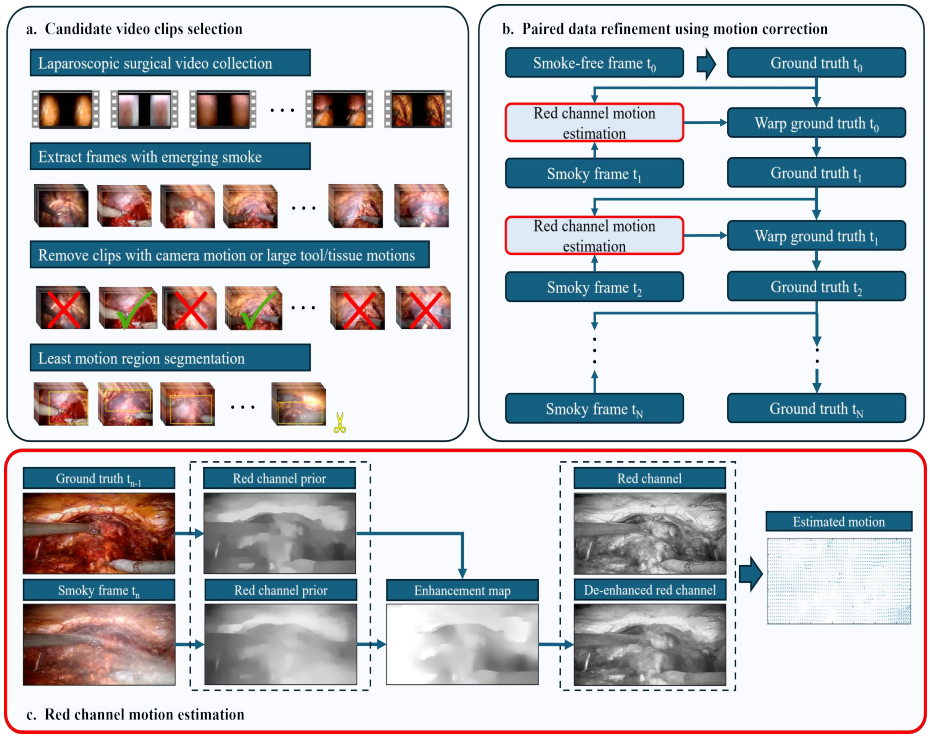

Fig. 1. Workflow for our database creation. a) Illustrates video clip selection for large motion rejection. b) Illustrates paired data refinement to address any remaining motion. c) A workflow for our motion estimation showcasing red channel priors.

We first manually screen laparoscopic videos to identify stationary sequences with emerging smoke, focusing on excluding large motion. A set of surgical videos recorded during robotic-assisted abdominal surgeries was obtained, chosen for their stability provided by mechanically held cameras with minimal camera motion during cauterization. Additionally, the chosen surgical scenario is prostatectomy: due to the site's distant proximity from the heart and lungs, is minimally impacted by involuntary anatomical movements. We then manually identified all video sequences where smoke emerges clearly, typically lasting 1-2 seconds from the start of cauterization, to ensure limited motion perturbed by tools and anatomies. These video segments were manually inspected to further reject clips based on the following criteria: 1) visible motion of the surgical tools or soft tissues, 2) visible camera motion, and 3) presence of dissected tissues. Finally, we conducted an additional round of visual inspection on the selected video clips to segment regions with minimal motion, excluding areas with visible motion and deformation. For our surgical video with spatial dimensions of 700×350 pixels, we defined "visible motion" as a tolerance of 5 pixels. This segmentation was consistently applied to all frames in the selected video sequence. To facilitate the visual inspection of local motion caused by the human operator, each pair of temporally adjacent video frames was converted into an animated GIF. This step yielded a set of candidate video segments each having an initial smoke-free frame serving as the potential "ground truth" for subsequent paired images with smoke. A graphical workflow is given in Fig. 1(a).

3.2 Motion correction using red channel prior

(a) (b) (c)

Fig. 2. Illustration of motion correction error when computing optical flow directly between smoke-free and smoky frames (a) smoky current frame (b) smoke-free previous frame(c) erroneous warping of previous smoke-free frame to match current frame

Video frames within the candidate video clip are not completely stationary, exhibiting small and continuous motion of the soft tissue and surgical instruments. While one may attempt to apply 2D deformable registration to warp the initial smoke-free frame to align with subsequent smoky images, the presence of surgical smoke makes this approach particularly challenging. As shown in Fig. 2, if the smoke-free image is warped using optical flow to match the smoky

image, large warping errors would occur. To circumvent this problem, we propose to employ only the red channel image to facilitate motion correction. Our observation is that the red channel is the least affected and degraded colour by surgical smoke compared to the other colour channels. This may be attributed to the longer wavelength of red light, which allows it to penetrate atmospheric conditions more effectively than the shorter wavelengths of blue or green light, causing the red light to scatter less when it encounters particles suspended in the air [2]. Since the red channel is also the dominant colour for surgical images [26], using it for tracking is advantageous as the red channel contains more background information with less degradation from smoke. As the max channel is commonly used to compute the illumination map for each image [3], smoke in the red channel can be considered as illumination differences between smoky and smoke-free images. Thus, we propose equalizing the illumination and "de-enhancing" the red channel of smoky images for robust motion correction. To facilitate the red channel de-enhancement, we first extract the red channel from the current smoky frame I and the smoke-free ground truth from the previous time frame G. We then construct the red channel prior map ${S_I}^*$ and ${S_G}^*$ for I_r and G_r, respectively, using the structural images [27]:

$$ {S_I}^* = \arg\min_{S_I} \frac{1}{\rho} ||I_r - S_I||_F^2 + ||(I_r * g_\sigma) \odot \nabla S_I||_1 \tag{1} $$

$$ {S_G}^* = \arg\min_{S_G} \frac{1}{\rho} ||G_r - S_G||_F^2 + ||(G_r * g_\sigma) \odot \nabla S_G||_1 \tag{2} $$

where $\rho > 0$ is a regularization parameter, $||\cdot||_F$ and $||\cdot||$ represent the Frobenius norm and l_1 norm, g_σ represents Gaussian kernel with standard deviation σ, and $\odot$ denotes Hadamard product. The de-enhancement map E can be obtained by:

$$ E(x) = \frac{\max_{x \in \Omega} S_G^*(x)}{\max_{x \in \Omega} S_I^*(x)} \tag{3} $$

where Ω is a region centered at pixel x. The de-enhanced red channel for a smoky image is obtained by $I_r^* = E \odot I_r$. The motion field D^* estimated by TV-L1 optical flow is obtained by Zach's approach [29]:

$$ D^* = \arg\min_{D} \sum_{x \in \Omega} (|G_r(x) - I_r^*(x + D(x))| + |\nabla D|) \tag{4} $$

The motion field D^* is then used to warp G to obtain the corresponding smoke-free ground truth for I. For each sequence, the ground truth at time t_n is obtained by warping the initial smoke-free frame at t_0. The workflow for motion correction and red channel de-enhancement is shown in Fig. 1(b) and (c). Human inspection remains the last safeguard to discard the frame or the entire dataset when there is any visible motion between the paired data.

4 Benchmark Dataset

A set of surgical videos was collected from a previous study of robotic-assisted laparoscopic radical prostatectomy performed using a da Vinci Si surgical system. In total, we reviewed 63 surgical recordings with an average of 37 minutes per video, and 32 candidate clips were identified after the first stage of screening. Among 32 candidates, 26 sequences were successful in motion correction, with no visible misalignment between paired images, and 5 more sequences were eventually discarded as the smoke was too thin to be significant. Each sequence contains varying levels of smoke from light to heavy, including the more challenging cases of non-homogeneous smoke containing suspended particles. Ultimately, our current dataset consists of 21 video sequences and 961 pairs of smoky images and their corresponding smoke-free ground truths, constituting less than 0.03 % of the entire reviewed video frames. Three human operators were involved in the reviewing process and a consensus was reached for the final paired dataset.

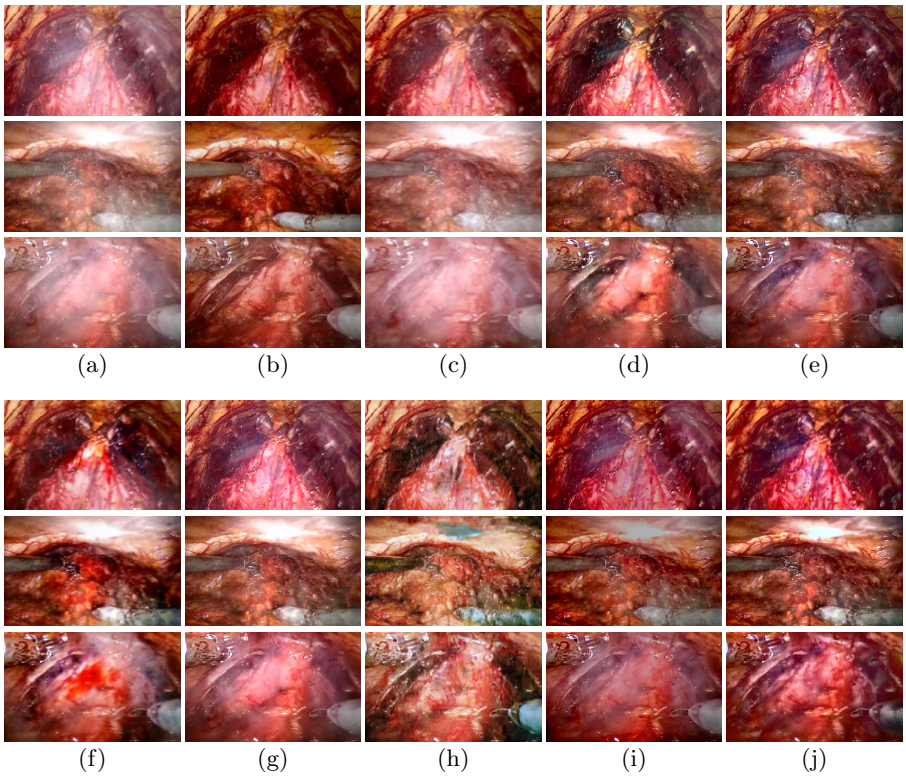

Fig. 3. De-smoking results comparison examples (a) Smokey images (b) Smoke-free ground truth (c) M1 (d) M2 (e) M3 (f) M4 (g) M5 (h) M6 (i) M7 (j) M8

Table 1. Quantitative comparison of 8 de-smoking methods over 961 images

Method	Approach	Train data	SSIM ↑	PSNR ↑	CIEDE-2000 ↓
M1 [12]	CycGan	Unpaired	0.83 ± 0.14	17.97 ± 4.98	11.70 ± 7.49
M2 [13]	CNN	Synthetic	0.88 ± 0.11	19.95 ± 3.94	7.93 ± 5.51
M3 [17]	CycGan	Unpaired	0.86 ± 0.10	19.44 ± 3.40	8.67 ± 4.10
M4 [15]	CNN	Synthetic	0.86 ± 0.08	19.74 ± 3.58	8.42 ± 4.15
M5 [16]	ViT	Synthetic	0.88 ± 0.14	20.80 ± 6.23	8.27 ± 6.98
M6 [6]	ViT	Outdoor	0.83 ± 0.08	20.29 ± 4.19	9.45 ± 4.94
M7 [20]	Variational	–	0.87 ± 0.09	18.36 ± 2.29	9.37 ± 3.21
M8 [9]	Analytical	–	0.86 ± 0.11	18.77 ± 3.68	9.25 ± 5.42

4.1 Benchmark Performance

Using our *in vivo* paired dataset, we compare recent de-smoking methods to establish a benchmark for future study, including two CycleGan-based methods, two CNN-based methods, two vision transformer (ViT) based methods, and two non-learning-based methods. For learning-based approaches, we compared methods with open source availability: (M1) a CycleGan-based unpaired method trained using inter-channel discrepancies and dark channel prior (DCP) [12], (M2) an image translation-based method with DCP guidance mask [13], (M3) A two-stage method combining pre-trained image translation and CycleGan [17], (M4) A image translation network utilizing SSIM and perceptual loss [15], (M5) An improved ViT with modified network architecture and spatial information aggregation scheme [16], (M6) A ViT-based method with uncertainty feedback for refinement by [6]. Although M5 and M6 are not trained on surgical scenes, they are the current lead for the homogenous high resolution dehaze dataset and outdoor non-homogeneous smoke dataset respectively, representing SOTA methods for natural scenes. For non-learning methods, we studied: (M7) a variational smoke separation algorithm with a smoke veil prior model [20], and (M8) a Poisson fusion-based defogging algorithm [9]. For evaluation metrics, we use peak signal-to-noise ratio (PSNR), structural similarity index (SSIM) [24], and colour difference formula (CIEDE-2000) [14]. Representative qualitative comparison examples are given in Fig. 3 including homogenous and non-homogenous smoke with a comprehensive quantitative evaluation given in Table 1. From Fig. 3, all methods are capable of removing smoke from *in vivo* images to certain degrees, especially for homogeneous smoke, and all methods seem to be less effective for scenes with non-homogeneous smoke and particles. Colour distortion and detail degradation are also observed, especially when smoke becomes heavy. In particular, M2 [13] and M5 [16] seem to produce the best results from visual inspection, striking a good balance between smoke removal and colour preservation. Based on the quantitative comparison in Table. 1, methods M2 [13] and M5 [16] have the highest SSIM and PSNR while causing less colour loss by CIEDE-2000 metric.

5 Conclusion and Future work

In this paper, we present the first paired dataset, *i.e.* paired images with and without surgical smoke, for laparoscopic image de-smoking techniques. We detailed the challenges of creating such a dataset using *in vivo* surgical videos and presented a novel methodology based on motion correction in the presence of surgical smoke. Moreover, our dataset contains consecutive video frames, making it suitable for evaluating an algorithm's performance consistency and stability over time, providing a mechanism to evaluate video- or sequence-based algorithms. Comparative studies confirmed the ability of current methods to remove smoke under surgical scenarios and revealed their limitations in dealing with non-homogeneous smoke and in preserving colour and detail. These findings suggest areas for future research and potential improvements in de-smoking techniques. The limitations of our work include 1) Our dataset primarily consists of video sequences with relatively stationary scenes, which may not be representative of all surgical scenarios, and 2) Our current approach for constructing this dataset relies on significant manual inspection of surgical videos, which is time-consuming and thus limits the expansion of the dataset. Immediate future work includes developing a deep-learning-based content recognition network to expedite the process and expanding the size of the dataset.

Disclosure of Interests. The authors have no competing interests to declare that are relevant to the content of this article.

References

1. Carbajo-Rodríguez, H., Aguayo-Albasini, J.L., Soria-Aledo, V., García-López, C.: Surgical smoke: risks and preventive measures. Cirugía Española (English Edition) **85**(5), 274–279 (2009)
2. Chabok, M., Millington, A., Hacker, J.M., McGrath, A.J.: Visibility through the gaseous smoke in airborne remote sensing using a DSLR camera. In: Themistocleous, K., Hadjimitsis, D.G., Michaelides, S., Papadavid, G. (eds.) Fourth International Conference on Remote Sensing and Geoinformation of the Environment (RSCy2016). vol. 9688, p. 96880Q. International Society for Optics and Photonics, SPIE (2016)
3. Guo, X., Li, Y., Ling, H.: Lime: Low-light image enhancement via illumination map estimation. IEEE Transactions on Image Processing **26**(2), 982–993 (2017)
4. He, C., Li, K., Xu, G., Yan, J., Tang, L., Zhang, Y., Wang, Y., Li, X.: HQG-Net: Unpaired medical image enhancement with high-quality guidance. IEEE Transactions on Neural Networks and Learning Systems pp. 1–15 (2023)
5. Hong, T., Huang, P., Zhai, X., Gu, C., Tian, B., Jin, B., Li, D.: MARS-GAN: Multilevel-feature-learning attention-aware based generative adversarial network for removing surgical smoke. IEEE Transactions on Medical Imaging **42**(8), 2299–2312 (2023)
6. Jin, Y., Yan, W., Yang, W., Tan, R.T.: Structure representation network and uncertainty feedback learning for dense non-uniform fog removal. In: Asian Conference on Computer Vision. pp. 155–172. Springer (2022)

7. Lawrentschuk, N., Fleshner, N.E., Bolton, D.M.: Laparoscopic lens fogging: a review of etiology and methods to maintain a clear visual field. Journal of Endourology **24**(6), 905–913 (2010)
8. Li, R., Tan, R.T., Cheong, L.F., Aviles-Rivero, A.I., Fan, Q., Schonlieb, C.B.: Rainflow: Optical flow under rain streaks and rain veiling effect. In: Proceedings of the IEEE/CVF international conference on computer vision. pp. 7304–7313 (2019)
9. Luo, X., McLeod, A.J., Pautler, S.E., Schlachta, C.M., Peters, T.M.: Vision-based surgical field defogging. IEEE Transactions on Medical Imaging **36**(10), 2021–2030 (2017)
10. Maier-Hein, L., et al.: Comparative validation of single-shot optical techniques for laparoscopic 3-d surface reconstruction. IEEE Transactions on Medical Imaging **33**(10), 1913–1930 (2014)
11. Narasimhan, S.G., Nayar, S.K.: Vision and the atmosphere. International Journal of Computer Vision **48**(3), 233–254 (2002)
12. Pan, Y., Bano, S., Vasconcelos, F., Park, H., Jeong, T.T., Stoyanov, D.: DeSmokeLAP: improved unpaired image-to-image translation for desmoking in laparoscopic surgery. International Journal of Computer Assisted Radiology and Surgery **17**(5), 885–893 (2022)
13. Salazar-Colores, S., Jiménez, H.M., Ortiz-Echeverri, C.J., Flores, G.: Desmoking laparoscopy surgery images using an image-to-image translation guided by an embedded dark channel. IEEE Access **8**, 208898–208909 (2020)
14. Sharma, G., Wu, W., Dalal, E.N.: The CIEDE2000 color-difference formula: Implementation notes, supplementary test data, and mathematical observations. Color Research & Application: Endorsed by Inter-Society Color Council, The Colour Group (Great Britain), Canadian Society for Color, Color Science Association of Japan, Dutch Society for the Study of Color, The Swedish Colour Centre Foundation, Colour Society of Australia, Centre Français de la Couleur **30**(1), 21–30 (2005)
15. Sidorov, O., Wang, C., Cheikh, F.A.: Generative smoke removal. In: Machine Learning for Health Workshop. pp. 81–92. PMLR (2020)
16. Song, Y., He, Z., Qian, H., Du, X.: Vision transformers for single image dehazing. IEEE Transactions on Image Processing **32**, 1927–1941 (2023)
17. Su, X., Wu, Q.: Multi-stages de-smoking model based on CycleGAN for surgical de-smoking. International Journal of Machine Learning and Cybernetics **14**(11), 3965–3978 (2023)
18. Venkatesh, V., Sharma, N., Srivastava, V., Singh, M.: Unsupervised smoke to desmoked laparoscopic surgery images using contrast driven Cyclic-DesmokeGAN. Computers in Biology and Medicine **123**, 103873 (2020)
19. Vishal, V., Venkatesh, V., Lochan, K., Sharma, N., Singh, M.: Unsupervised desmoking of laparoscopy images using multi-scale desmokenet. In: Blanc-Talon, J., Delmas, P., Philips, W., Popescu, D., Scheunders, P. (eds.) Advanced Concepts for Intelligent Vision Systems. pp. 421–432. Springer International Publishing, Cham (2020)
20. Wang, C., Alaya Cheikh, F., Kaaniche, M., Beghdadi, A., Elle, O.J.: Variational based smoke removal in laparoscopic images. Biomedical Engineering Online **17**(1), 1–18 (2018)
21. Wang, C., Zhao, M., Zhou, C., Dong, N., Khan, Z.A., Zhao, X., Cheikh, F.A., Beghdadi, A., Chen, S.: Smoke veil prior regularized surgical field desmoking without paired in-vivo data. Computers in Biology and Medicine **168**, 107761 (2024)

22. Wang, D., Qi, J., Huang, B., Noble, E., Stoyanov, D., Gao, J., Elson, D.S.: Polarization-based smoke removal method for surgical images. Biomedical Optics Express **13**(4), 2364–2379 (2022)
23. Wang, F., Sun, X., Li, J.: Surgical smoke removal via residual swin transformer network. International Journal of Computer Assisted Radiology and Surgery **18**(8), 1417–1427 (2023)
24. Wang, Z., Bovik, A.C., Sheikh, H.R., Simoncelli, E.P.: Image quality assessment: from error visibility to structural similarity. IEEE Transactions on Image Processing **13**(4), 600–612 (2004)
25. Wei, Y., Zhang, Z., Wang, Y., Xu, M., Yang, Y., Yan, S., Wang, M.: Deraincyclegan: Rain attentive cyclegan for single image deraining and rainmaking. IEEE Transactions on Image Processing **30**, 4788–4801 (2021)
26. Xia, W., Chen, E.C.S., Pautler, S.E., Peters, T.M.: A global optimization method for specular highlight removal from a single image. IEEE Access **7**, 125976–125990 (2019)
27. Xu, L., Yan, Q., Xia, Y., Jia, J.: Structure extraction from texture via relative total variation. ACM Transactions on Graphics (TOG) **31**(6), 1–10 (2012)
28. Yang, Y., Wang, C., Liu, R., Zhang, L., Guo, X., Tao, D.: Self-augmented unpaired image dehazing via density and depth decomposition. In: Proceedings of the IEEE/CVF conference on computer vision and pattern recognition. pp. 2037–2046 (2022)
29. Zach, C., Pock, T., Bischof, H.: A duality based approach for realtime tv-l 1 optical flow. In: Pattern Recognition: 29th DAGM Symposium, Heidelberg, Germany, September 12-14, 2007. Proceedings 29. pp. 214–223. Springer (2007)
30. Zhang, J., Huang, W., Liao, X., Wang, Q.: Progressive frequency-aware network for laparoscopic image desmoking. In: Chinese Conference on Pattern Recognition and Computer Vision (PRCV). pp. 479–492. Springer (2023)
31. Zhu, J.Y., Park, T., Isola, P., Efros, A.A.: Unpaired image-to-image translation using cycle-consistent adversarial networks. In: Proceedings of the IEEE international conference on computer vision. pp. 2223–2232 (2017)